Effect of alloying on the phase stability and elastic properties of $L1_2$ Cu_3Pt crystal structure

Tiny Mathibeng[1,3*], *Hein* Möller[1,2], *Maje* Phasha[2] and *Alain* Mwamba[2]

[1]University of Pretoria, Cnr Lynnwood and University Roads Hatfield Pretoria, South Africa
[2]Advanced Materials Division, MINTEK, 200 Malibongwe Drive, Randburg, South Africa
[3]SADPMR, 38 Bonaero Drive, Kempton Park, South Africa

Abstract. The alloying effect of three elements, namely Al, Cr and Zn, on the Pt site of $L1_2$ Cu_3Pt phase was investigated using DFT (density functional theory) based first-principle calculations in attempt to stabilize it in the form of $L1_2$ $Cu_3Pt_{1-x}Y_x$ ternary alloy. On the basis of phase stability and elastic properties, the substitution behaviour of all three alloying elements were compared with properties of thermodynamically sluggish Cu_3Pt phase. The calculated heats of formation reveal that the thermodynamic phase stability is gradually enhanced with increasing content of aluminium alloying and diminished with increasing content of zinc and chromium. In this current work, the stress-strain approach was used according to Hooke's law to calculate elastic properties such as elastic constants, Young's modulus E, shear modulus G, bulk modulus B and Poisson's ratio v, as they play an important role to investigate the resulting mechanical properties. The calculated results show that alloying with all three elements maintains the mechanical stability criteria of cubic crystals. Considered $L1_2$ $Cu_3Pt_{1-x}Y_x$ ternary alloys exhibit the most ductile character with Al addition, followed by Cr, whereas introduction of Zn yielded lowest ductility at higher compositions.

1 Introduction

Lately, the alloys belonging to Cu-Pt system have received immense attention in research due to their importance in earmarked applications such as proton exchange membrane fuel cells (PEMFCs) as catalyst [1-4] as well as in smart thermoelectric generators (TEG) for harvesting waste energy [5]. It is reported that atomic ordering in Pt-M alloys (M: non-platinum group metals (PGMs) such as Cu, Ni, Fe, Co) improves catalytic performance and stability of the cathode through alteration of surface and electronic structure, resulting in efficient oxygen reduction reaction (ORR) and methanol oxidation reaction (MOR) in which the Pt poisoning resistance and durability is improved [3, 6, 7]. Recent successes in synthesis of Cu_3Pt alloy nanoframes with a core-shell structure which further enhanced the ORR catalytic activity have sparked more interest in the study of bimetallic alloys comprised of PGM and non-PGM [8-12]. This interest stems from the potential applications of such novel materials in energy

* Corresponding author: tinym@sadpmr.co.za; majep@mintek.co.za

storage and conversion such as hydrogen storage, hydrogen production, and active fuel cell catalysts [13]. These developments are also positive towards addressing one of the stumbling blocks hindering industrial rollout of fuel cells that use pure Pt as a cathode catalyst, which is its high cost which accounts for at least half of the overall PEMFC manufacturing cost [14].

On the other hand, ordered intermetallics constitute a unique class of materials that form long-range ordered (LRO) crystal structure below a critical temperature that is generally referred to as the critical order-disorder phase transition temperature [15, 16]. The interest in such materials emanate from their attractive properties such as high strength, stiffness, stability and oxidation resistance ideal for structural applications at elevated temperatures [15]. The thermodynamic stability of these compounds relates to their high bond strength brought about by ordering. As a result, the lower the thermodynamic stability corresponds to lower order-disorder phase transition temperature because it requires less amount of energy in the form of temperature to weaken the bond. Thus for $L1_2$ Cu_3Pt alloy to be suitable for structural applications, its thermodynamic stability needs to be increased so that the ordering temperature can be higher than 735 °C, shown in Figure 1. This figure shows the Cu-Pt alloy phase diagram redrawn from Hansen [17]. The literature shows that the Cu-Pt alloy system consists of different phases, a continuous solid solution phase and several ordered intermetallic phases at low temperatures. The Cu-Pt system is the only platinum-based system which takes up a unique long-range ordered rhombohedral $L1_1$-CuPt superlattice near 50% wt.% from FCC cubic disordered lattice below 812 ^{0}C Figure 1 [18]. $L1_2$-Cu_3Pt and one dimensional long-period structure (LPS) have been observed at 30 wt.% Pt composition. The congruent point for the order-disorder transition of the $L1_2$-Cu_3Pt phase appears around 16 wt.% Pt composition [18]. Additionally, the following phases were described, A1-disordered phase, $L1_2$-Cu_3Pt and $L1_1$-CuPt stable phases and $L1_2$-Cu_3Pt and $L1_0$ CuPt metastable phases in the Pt-Cu alloy [18].

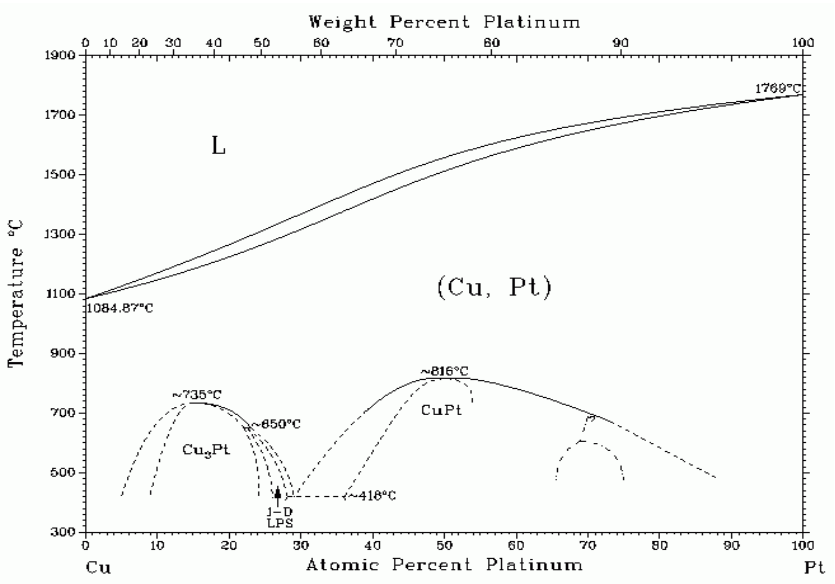

Fig. 1. Phase diagram of Cu-Pt (Copper Platinum) [17].

Therefore, the current work aims to investigate the effect of alloying on the phase stability and elastic properties of the $L1_2$ Cu_3Pt phase using DFT (density functional theory) based first-principle technique. Three elements, namely Al, Cr and Zn were chosen for substitution on the Pt site of $L1_2$ Cu_3Pt phase from a view-point of increasing stability, strength and

oxidation resistance in $L1_2$ $Cu_3Pt_{1-x}Y_x$ ternary compositions. The focus is on understanding how alloying affects structural and mechanical properties and identify which alloying element promotes potential use as catalyst or structural material.

2 Methodology

First principles modelling of $L1_2$ Cu_3Pt and ternary compositions was carried out using FCC supercells with space group #221(Pm-3m) consisting of 32 atoms and with the following structural compositions: $Cu_{24}Pt_7Al_1$, $Cu_{24}Pt_6Al_2$, $Cu_{24}Pt_7Zn_1$, $Cu_{24}Pt_6Zn_2$, $Cu_{24}Pt_7Cr_1$ and $Cu_{24}Pt_6Cr_2$ to represent 3.125 and 6.25 atomic percent (at. %) of the alloying element. All calculations in this work were performed using densify functional theory (DFT) based CASTEP code embedded in Materials Studio software package [19]. Robust Vanderbilt ultrasoft pseudopotentials [20] were used to describe the ion-electron interaction within the generalized gradient approximation (GGA) [21] of Perdew-Burke-Ernzerhof (PBE) [22]. A plane wave energy cutoff of 500 eV and k-points set of 6x6x6 were sufficient to converge the total energy of the considered systems. Effects of alloying on the phase stability and elastic properties of $L1_2$ $Cu_3Pt_{1-x}Y_x$ (Y=Al, Zn, Cr) were determined from the ground-state structures optimized using the Brayden-Fletcher-Goldfarb-Shanno (BFGS) minimization scheme. The convergence criterion of less than 1×10^{-5} eV/atom, the maximum residual forces of 0.03 eV/Å, maximum residual bulk stress of 0.05 GPa and maximum atomic displacement of 1×10^{-3}Å were utilized.

2.1 Phase stability

In order to determine the thermodynamic stability, heats of formation were calculated from equation 1 below:

$$H_F = \frac{1}{n}E_{Total}^{Cu_3Pt_{1-x}Y_x} - \left[(0.25-x)E_{Solid}^{Pt} + xE_{Solid}^{Y} + 0.75E_{Solid}^{Cu}\right] - - - - - [1]$$

where $E_{Total}^{Cu3Pt1-xYx}$ is the total energy of the alloy, E_{Solid}^{Pt}, E_{Solid}^{Cu} and E_{Solid}^{Y} are the total energies of the ground-state structures of elemental Pt, Cu and corresponding alloying elements. Whereas *x* and *0.25-x* refer to the fractional concentrations of the constituent elements, the total number of atoms in the superstructure is represented by *n*.

2.2 Elasticity properties

The stress-strain relation may be used to distinguish the elastic and plastic regimes of solid materials. The elastic moduli are the fundamental physical parameters which establish the stress-strain relation in the elastic regime. For an isotropic polycrystalline solid, the two independent elastic parameters are the bulk modulus (*B*) and the shear modulus (*G*). The ratio of *B/G* predicts the brittleness of metals depending on the threshold value of 1.75 (ductile if above 1.75). For the cubic structures, only three elastic constants, corresponding to C_{11}, C_{12}, and C_{44}, are independent. The mechanical stability criteria of cubic crystals are given by expressions shown in equation 2, along side other mechanical property expressions in equation 3 with subscripts V, R, and H denoting Voigt, Reuss, and Hill averages, respectively.

$$C_{11} > 0,\ C_{44} > 0, \qquad C_{11} - C_{12} > 0, \qquad C_{11} + 2C_{12} > 0 \ - - - - - [2]$$

$$B_V = B_R = \frac{1}{3}(C_{11} + 2C_{12}),\ C' = \frac{C_{11} - C_{12}}{2},\ G_H = \frac{G_V - G_R}{2},\ E = \frac{9B_H G_H}{3B_H + G_H},$$
$$U = 0.5\left(\frac{3B_H - 2G_H}{3B_H + G_H}\right) \quad ----------[3]$$

3 Results and discussion

3.1 Phase stability

Figure 2(a) and (b) presents the calculated lattice constants and formation energies, respectively, of binary $L1_2$ Cu_3Pt and $Cu_3Pt_{1-x}Y_x$ ternary alloys plotted against alloying element composition. As shown in Figure 2(a), the lattice constant increases with introduction of 3.125 at.% of any of the three alloying elements and decreases gradually upon further increase in composition to 6.25 at.%. The effect of Al and Zn addition on the lattice parameter is almost similar while Cr addition causes the least lattice expansion at 3.125 at.% and highest contraction at 6.25 at.%. The resulting trend corresponds to the atomic sizes of individual alloying elements. From the heats of formation results presented in Figure 2(b), it is evident that Cr addition leads to sharp reduction in thermodynamic stability while Al addition show the opposite trend in which stability increased. On the other hand, thermodynamic stability remains constant on introduction of Zn. The interpretation of the above stability trend is drawn on the basis that the heats of formation predict the phase to be thermodynamically stable when its value is negative ($H_f<0$), so a higher phase stability is indicated by the higher negative value. Formation energy of a binary Cu_3Pt alloy was calculated to benchmark the formation of ternary alloys in order to determine the effect of doping elements on the platinum-site on the phase stability. Consequently, the current results predict Al addition to be most effective in increasing the thermodynamic stability of $L1_2$ Cu_3Pt alloy with likelihood to increase the corresponding order-disorder phase transformation temperature [23], thus promoting its viability for being considered for structural applications provided the corresponding mechanical properties are also higher than those of unalloyed binary $L1_2$ Cu_3Pt alloy.

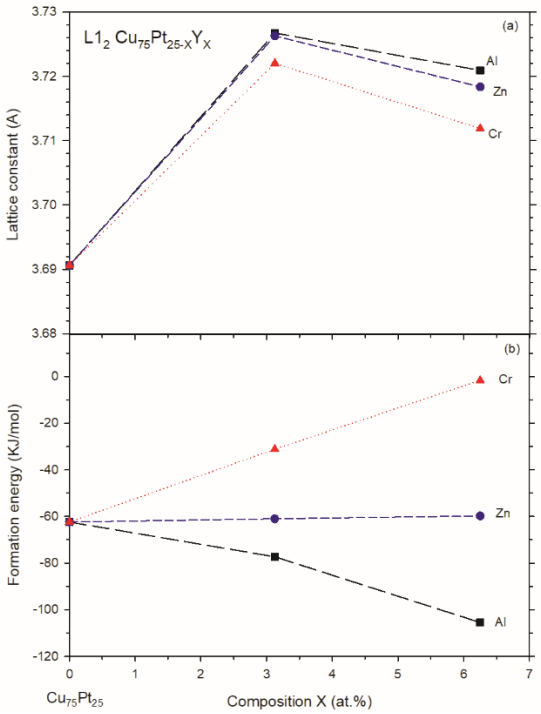

Fig. 2. Lattice constant (a) and Formation energy (b) of L1$_2$ Cu$_3$Pt$_{1-x}$Y$_x$ ternary alloys

3.2 Elastic properties

The response of a crystal structure to external force is determined by elastic constants, hence in this current work it was important to investigate elastic properties according to stress-strain approach.

Figure 3 presents the predicted elastic constants C_{11}, C_{12}, and C_{44} of L1$_2$ Cu$_3$Pt$_{1-x}$Y$_x$ compositions plotted against composition of respective alloying element Al, Zn and Cr in (a), (b) and (c), respectively. The effect of alloying trend on these elastic constants is similar for Al and Cr, where there is an initial increase of C_{11} and C_{12} at 3.125 at.% composition and a decrease thereafter at 6.25 at.%, whereas C_{44} increases gradually with increasing alloying elements for all three metals. As shown in Figure 3(b), both C_{11} and C_{12} decrease with Zn addition. Of importance is how these elasticity trends impact on the resulting elastic properties, as shown in Figure 4. It follows from Figure 4(a) that although the addition of all three alloying element maintains the mechanical stability criterion given in equation 2, the value of the tetragonal shear modulus (C'), which measures the degree of mechanical stability of a crystal, first drops at 3.125 at.% for all three alloying elements and increase thereafter at 6.25 at.% for Al and Zn while it continues to decrease in the case of Cr. These results suggest higher content of Al and Zn to be effective in increasing the mechanical stability of L1$_2$ Cu$_3$Pt alloy. Furthermore, the above proposed ternary alloy compositions show highest Young's and Shear moduli amongst considered ternary compositions but these predicted elastic properties are much lower than those of unalloyed L1$_2$ Cu$_3$Pt alloy, as shown in Table I. These moduli are directly linked to material strength. Thus the obtained inferior mechanical propeties of considered ternary compositions do not promote the potential use of these alloys in electrocatalytic applications. These moduli are directly linked to material strength. Therefore a combination as shown in Figure 4(a) and (b) for Al and Zn, the decrease and increase in C'

corresponds with increase and decrease in B/G_H, which is a measure of ductility. However, this direct correlation is violated in the case Cr. Addition of Zn at 6.25 at.% results in embrittled material. Although the embrittlement noticed in $Cu_{24}Pt_6Zn_2$ has a negative consequence on formability using conventional routes, the advent of additive manufacturing (AM) may presents an opportunity in terms of processing this alloy composition. Moreover, as shown in Table 1, this alloy possess the lowest Poisson's ratio, an indication of improved wear properties such as erosion resistance compared to unalloyed binary $L1_2$ Cu_3Pt alloy. Therefore, despite $Cu_{24}Pt_6Zn_2$ composition showing the highest stiffness amongst all considered ternary compositions, it is inferior to unalloyed $L1_2$ Cu_3Pt, thus rendering studied ternary alloy compositions unsuitable for structural applications.

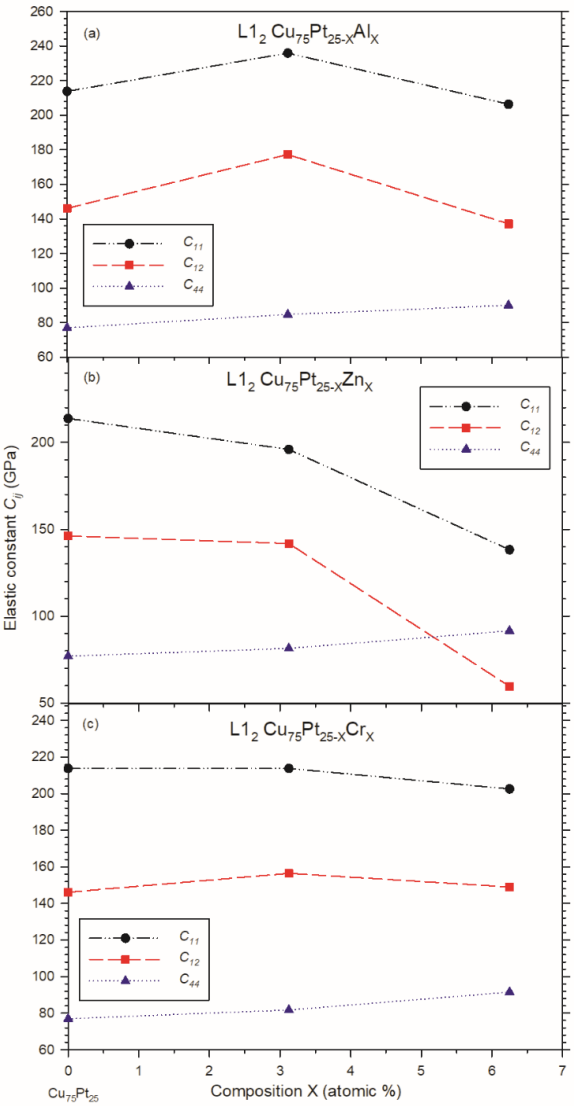

Fig. 3. Predicted elastic constants of $L1_2$ $Cu_3Pt_{1-x}Y_x$

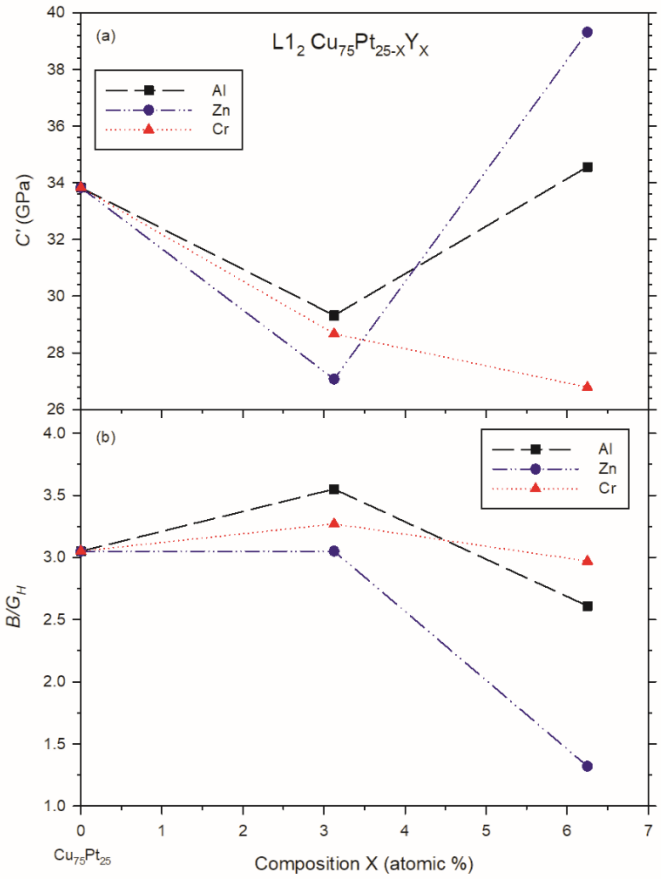

Fig. 4. Predicted elastic moduli of $L1_2$ $Cu_3Pt_{1-x}Y_x$

Table 1. Calculated mechanical properties of $L1_2$ $Cu_3Pt_{1-x}Y_x$

Composition	Bulk Modulus *B* (GPa)	Young' Modulus *E* (GPa)	Shear Modulus G_H (GPa)	Poisson's ratio U (GPa)
$Cu_{24}Pt_8$	232.64	182.06	94.14	0.322
$Cu_{24}Pt_7Al_1$	196.74	83.79	62.53	0.429
$Cu_{24}Pt_6Al_2$	160.17	96.74	67.82	0.399
$Cu_{24}Pt_7Cr_1$	175.55	81.57	60.51	0.423
$Cu_{24}Pt_6Cr_2$	166.84	76.24	65.63	0.424
$Cu_{24}Pt_7Zn_1$	159.85	76.87	59.69	0.420
$Cu_{24}Pt_6Zn_2$	85.80	102.31	70.65	0.301

4 Conclusion

The thermodynamic phase stability was gradually enhanced with increasing aluminium content, diminished with increasing chromium amount, and remained constant on zinc

addition. As a result, current work predicted addition of at least 6 at.% Al to be most effective in increasing the thermodynamic stability of $L1_2$ Cu_3Pt alloy with likelihood to increase the corresponding order-disorder phase transformation temperature. Alloying with 6 at.% Al and Zn on $L1_2$ $Cu_3Pt_{1-y}X_y$ ternary compositions yielded promising results in terms of mechanical properties, but these properties are inferior to those obtained for binary $L1_2$ Cu_3Pt alloy. Therefore, since the predicted strength, drawn from Young's and Shear moduli, of all ternary compositions considered in this study is much lower than that of binary $L1_2$ Cu_3Pt alloy, these ternary compositions are rendered unsuitable for both structural and electrocatalytic applications.

5 Acknowledgements

This work was mostly conducted at MINTEK's computer laboratory and supported by MINTEK, University of Pretoria And South African Diamond and Precious Metals Regulator. Furthermore, the gratitude is extended to the Centre for High-Performance Computing (CHPC) in Cape Town for allowing us to carry out the calculations using their remote computing resources.

References

1. X. Ren, Q. Lv, L. Liu, B. Liu, Y. Wang, A. Liu, and G. Wu, Sustain. Energy Fuels **4**, 15 (2020).
2. L. Ou, Comput. Theor. Chem. **1048**, 69 (2014).
3. H.Y. Kim, and S.H. Joo, J. Mater. Chem. A **8**, 8195 (2020).
4. L.D. Geoffrion, M. Jose-Yacaman, A. Lehr, S. Yang, J. Sanchez, J.J. Velazquez-Salazarb, and G. Guisbiers, Nanoscale Adv. **3**, 3746 (2021).
5. K. Tian and A. Tiwari, Sci. Rep. **9**, 31339| (2019).
6. X. Zhao, H. Cheng, L. Song, L. Han, R. Zhang, G. Kwon, L. Ma, S.N. Ehrlich, A.I. Frenkel, J. Yang, K. Sasaki, and H.L. Xin, ACS Catalysis **11**, 184 (2021).
7. G. Saravanan, R. Khobragade, L.C. Nagar, and N. Labhsetwar, RSC Advances **6**, 85634 (2016).
8. R. Yang, P. Strasser, and M.F. Toney, J. Phys. Chem. C **115**, 9074 (2011).
9. L. Han, H. Liu, P. Cui, Z. Peng, S. Zhang, and J. Yang, Sci. Rep. **4**, 6414 (2014).
10. F. Nosheen, T. Anwar, A. Siddique, and N. Hussain, Front. Chem. **7**, 456 (2019).
11. L. Bai, and Y. Bai, Nanopart. Res. **20**, 24 (2018).
12. C. Chen et al., Science **343**, 1339 (2014).
13. A.E. Hughes, N. Haque, S.A. Northey, and S. Giddey, Resources **10**, 93 (2021).
14. L. Mølmen, K. Eiler, L. Fast, P. Leisner, and E. Pellicer, APL Materials **9**, 040702 (2021).
15. A.O. Mekhrabov, and M.V. Akdeniz, Metall. Trans. A **34A**, 733 (2003).
16. M. Yildirim, M.V. Akdeniz, and A.O. Mekhrabov, Metall. Trans. A **43A**, 1809 (2012).
17. S. Mehmood, E.U. Klotz, and G. Potlaccher, Metall. Trans. A **43A**, 5029 (2012).
18. T. Abe, B. Sundman, and H. Onodera, JPED **27**, 5 (2006).
19. S. Clark, M.D. Segall, C.J. Pickard, P.J. Hasnip, M.I.J. Probert, K. Refson, and M.C. Payne., Zeitschrift fuer Kristallographie **220**, 567 (2005).

20. D. Vanderbilt. Phys. Rev. B **41**, 7892 (1990).
21. J.P. Perdew, and Y. Wang. Phys. Rev. B **45,** 13244 (1992).
22. J.P. Perdew., K. Burke, and M. Ernzerhof. Phys. Rev. Lett. **77,** 3865 (1997).
23. K. Matsui, and M. Takahashi, Phil. Mag. Lett. **77,** 49 (1998).